

A feasibility study into prognostics for the main bearing of a wind turbine

Shane Butler¹, Frank O'Connor², Des Farren² and John. V. Ringwood¹

Abstract—Maintenance for wind turbines, particularly offshore turbines, presents a significant cost component to wind farm operators. The main bearing, which supports the low-speed shaft, is one of the major wind turbine system components. Since maintenance is confined to suitable weather windows, which are unpredictable, there is a need for decision support tools to ensure that maintenance is carried out in a timely way, but also at minimum cost and with minimum turbine downtime. This paper presents a methodology for the estimation of the remaining useful life (RUL) of the main bearing for a commercial wind turbine. A residual model is used to highlight potentially faulty behaviour, which is then post processed to provide a suitable signal for extrapolation using particle filters. The RUL is then effectively specified as a probability distribution which narrows as the failure point is approached, providing an estimate of RUL and a confidence measure. Our results suggest that RULs beyond 30 days can be reasonably estimated.

I. INTRODUCTION

Over the past decade, the deployed wind generating capacity worldwide has increased rapidly. By the end of 2010, wind generating capacity reached approximately 196,630 MW [1]. In addition, the size and generating capacity of individual wind turbines also continues to increase, with turbines of capacity >5MW becoming standard in offshore wind farms. Over time, the constantly changing loads imparted by changing wind speeds and directions, as well as asymmetric loading due to the large vertical span of the turbine rotors, generate significant stresses on turbine blades, which is transferred to the transmission system. For offshore wind farms, studies have suggested that maintenance costs are about 20 to 25% of the total income generated, and that a considerable percentage of these costs are due to unexpected equipment failure, which require corrective maintenance [2].

With the clear imperative to minimise maintenance costs and maximise availability, condition monitoring for wind turbines is an area of widespread research activity. Researchers and practitioners have been investigating condition monitoring solutions for many of the different components on wind turbines, using a wide variety of different approaches. A number of publications are available which provide a review of the different techniques and approaches which have been investigated [3], [4], [5].

Wind turbines contain multiple rotating components, including the main shaft, multi-stage gearbox, and generator.

¹S. Butler and J.V. Ringwood are with the Dept. of Electronic Engineering at the National University of Ireland, Maynooth, County Kildare, Ireland.

²F. O'Connor and D. Farren are with ServusNet Informatics Ltd, National Software Centre, Mahon, Cork, Ireland.

As a result, vibration monitoring has been investigated for application to wind turbine condition monitoring and fault diagnostics [6], [7], with wavelet methods having widespread application due to their inherent ability to provide time-frequency resolution. This is important due to the variable-speed operation of wind turbines [8], [9]. Acoustic emissions (AE) analysis, designed to detect the stress waves generated by the rubbing of rotating components, has also been proposed for wind turbine condition monitoring [10], since the relatively low-speed operations for wind turbines can place limitations on vibration monitoring.

To address cracking and delamination in large (usually composite) wind turbine blades, electrical strain gauges, located at different stress points, have been used to monitor peak strains. The objective is to identify locations where structural damage may have occurred. More recently, fibre optic strain gauges have been employed [5], [11].

Wind turbine power curve analysis provides an indicator of overall wind turbine health [12]. Given the current wind conditions and air density, differences between the expected power output, as estimated by the power curve, and the actual power output are identified. The difference, which is often called the *power residual*, can be used to indicate overall blade condition [13], and gearbox faults [12].

In most modern wind turbines, supervisory control and data acquisition (SCADA) systems are now common. Some more recent SCADA systems also monitor overall vibration levels within critical components [14]. One of the primary drivers for using SCADA data for condition monitoring is that the data collection and sensor networks are already in place, which makes such approaches significantly cheaper. In contrast, comprehensive vibration monitoring and AE approaches require high-frequency data which might be sampled at up to 20 kHz. The costs of the required sensor network and the data collection, storage, and processing capabilities required to analyse and extract relevant features from the high-bandwidth raw vibration signals are significant. Furthermore, due to the high-bandwidth data required for advanced vibration monitoring, all significant signal processing and feature extraction must be performed locally at each turbine, with the extracted features and measurements then transmitted to a central location for further analysis and decision making [6]. As a result, the cost per turbine of installing such a system is often significant. SCADA data is also used to develop models which describe the fault-free behaviour of different turbine components. Differences between the estimated behaviour and observed behaviour can then be used to identify the presence of potential fault conditions.

A number of authors have considered such approaches for gearbox and generator components [15], [14].

This paper uses SCADA data to perform condition monitoring of the main bearing of a commercial wind turbine. A residual, based on a model of ‘normal’ main bearing temperature (MBT) behaviour, is evaluated, further processed and extrapolated into the future, using particle filters, to give an estimate of remaining useful life (RUL). While related studies, based on residual analysis, have been performed elsewhere on gearbox bearing temperature [14], [15] and generator [16], the main turbine bearing has received little attention. In addition, our method, based on particle filtering (and inspired by successful application elsewhere [17]) also provides statistical RUL estimation, not previously seen in the wind turbine industry.

II. AVAILABLE DATA AND PRE-PROCESSING

For this study, data from a large wind-farm was made available. For each turbine, the complete history of sensor information and turbine status information, for a period of 11-months, was available. The onboard SCADA system for each turbine records 10-minute averages of each monitored sensor variable. In addition, the maximum, minimum, and standard deviation of each of these sensor values, over each 10-minute period, is also recorded by the SCADA system. In addition to the values of the onboard sensors, status information, such as generator start and stop times, are also recorded by the SCADA system. Within the available data, just two turbines exhibited main bearing failure characteristics, which is the main reason that this paper represents a feasibility study rather than a comprehensive treatment.

A. Input variable selection

The objective here is to select a set of variables which maximise the diagnostic capabilities of the MBT residual emanating from the model built on normal operation and driven with the set of set of selected variables. While there are many objective procedural methods to select a set of explanatory variables, such as stepwise regression [18], these methods (usually based on linear regression) use modelling capability as an objective function. In our case, we are interested in maximising the diagnostic capability, so a broader approach to input variable selection was taken, essentially relying on multiple trials of various combinations of input variables, with diagnostic power as a criterion. This approach results in the following selection:

- **Main Shaft RPM.** The heat generated in the main bearing is, in general, a monotonic function of the main shaft RPM.
- **Hydraulic Brake Temperature.** The turbine brake is located on the high-speed shaft, which connects the gearbox to the generator, and analysis has demonstrated that, under fault-free conditions, the brake temperature is closely correlated with the main bearing temperature.
- **Hydraulic Brake Pressure.** The average hydraulic brake pressure over a ten-minute interval provides a measure of the brake friction applied to the high-speed

shaft which, in turn, generates friction within the main bearing, resulting in a response in the main bearing temperature

- **Blade Pitch Position.** All modern turbines employ pitch control to regulate rotor torque. With a constant main shaft RPM, the load experienced by the main bearing will be some function of the blade pitch position.

B. Ambient temperature compensation

Turbine sensor variables, and particularly temperature sensor variables, are a function of both the current operating conditions and the ambient temperature. Ideally, any correlation with ambient temperature should be removed from temperature measurements so that decision variables represent only the machine state, rather than ambient conditions. We employ a method suggested by Wiggelinkhuizen *et al* [19] which removes the linear relationship between main bearing temperature and ambient temperature. The effect of ambient temperature is highlighted at low rotational speeds, so data corresponding to rotor RPM values on the interval $[0.1, 1]$ were used to determine the relationship. Fig.1 shows the validity of a linear regression model. Fig.2 shows the

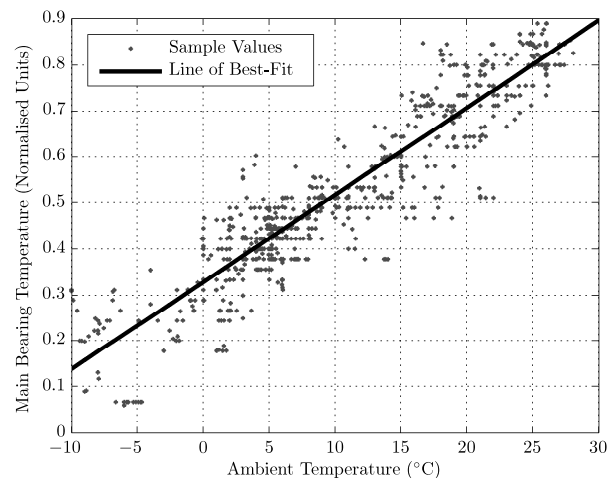


Fig. 1. Relationship between main bearing temperature and ambient temperature, under low-load conditions

effect of ambient temperature decorrelation on a typical main bearing temperature signal. The seasonal variation in ambient temperature is clear, with the main bearing temperature values are normalised, for confidentiality reasons.

III. RESIDUAL GENERATION AND FAULT DETECTION

In this section, we will develop a model of ‘normal’ operation for the main bearing of a turbine and use a signal derived from the model residual to identify the occurrence of a potential fault condition.

A. Modelling of normal operation

In previous similar studies [15], [14], multi-layer perceptron artificial neural networks have been widely employed for

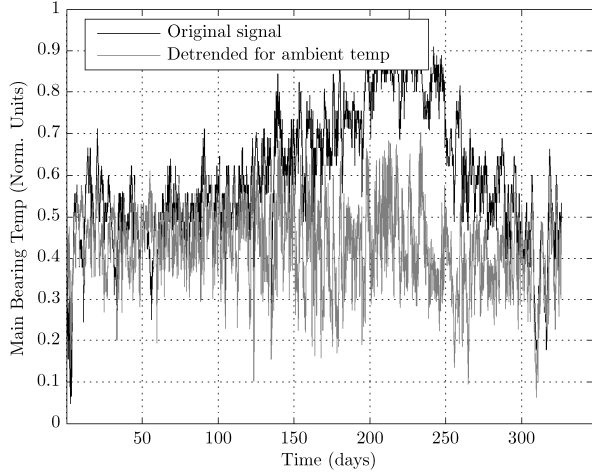


Fig. 2. Main bearing temperature: original signal and normalised for ambient temperature signal

modelling the fault-free behaviour of turbine components. In this study, a model of the form:

$$\hat{r}(k) = \sum_{i=1}^P w_i \phi_i(U) \quad (1)$$

is defined, where the $\phi(\cdot)$ form of a set of radial basis functions, with:

$$U = [r(k-1) \ u_1(k) \ u_1(k-1) \ u_2(k) \ u_3(k) \ u_4(k)]^T \quad (2)$$

where $\hat{r}(k)$ is the estimated main bearing temperature at time k , $r(k-1)$ is the actual main bearing temperature at time $k-1$. The u_i are defined as:

- u_1 : Main shaft RPM
- u_2 : Hydraulic brake temperature
- u_3 : Hydraulic brake pressure
- u_4 : Blade pitch position

Sparse Bayesian learning for the parameters (the w_i) was considered for a number of reasons:

- Sparse Bayesian learning models have excellent generalisation capabilities on unseen data, due to the low complexity representation (weights are driven to zero, where appropriate). Furthermore, the outputs generated by sparse Bayesian learning models are probabilistic, providing variance estimates on the generated predictions.
- Preliminary modelling studies demonstrated that it is not possible to develop a single model which could be used to describe fault-free behaviour across all turbines in a wind farm, highlighting the need for individualised ‘normal’ behaviour models. Therefore, a significant number of model need to be built and the fast marginal likelihood maximisation approach developed by Tipping *et. al* [20], provides extremely fast training.

Three fault-free turbines were randomly selected from the available data set. For each fault-free turbine, approximately

12,000 samples (from a total of 48,000), representing approximately 3 months of data, were selected for *model training*. Note that the data selected for training was taken from a different three month period for each turbine, to verify the insensitivity to ambient temperature. Each turbine model was tested on the remaining previously unseen samples for each turbine. Fig.3 shows the performance of the first fault-free turbine model over a typical 20-day period of previously unseen data. The distribution of the error signal for the

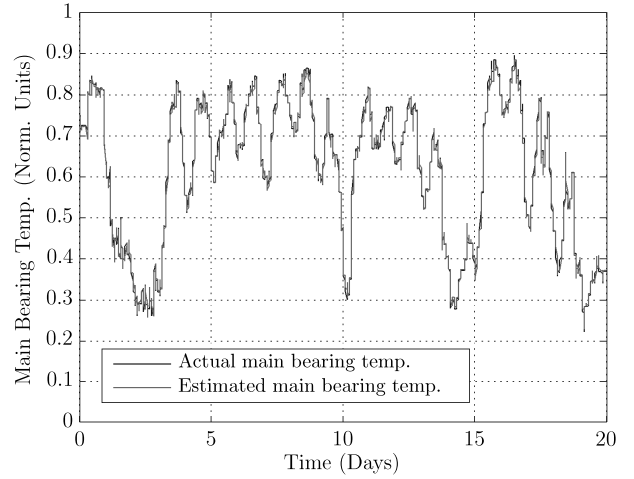


Fig. 3. Main bearing temperature estimation and generated residual signal (fault-free turbine)

second turbine, for the complete 8-months of test data, is plotted as a histogram in Fig.4. showing that the error is zero-mean and Gaussian.

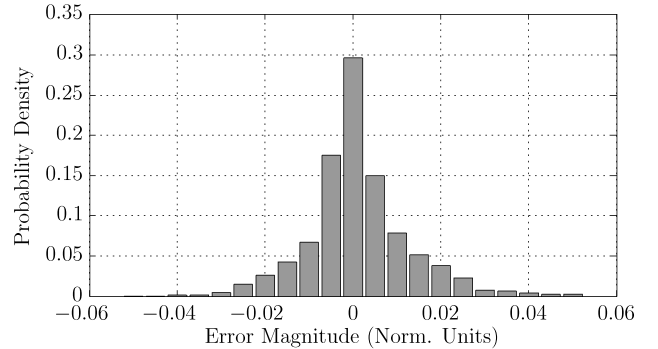


Fig. 4. Distribution of residual signal between estimated and actual main bearing temperature (fault-free turbine)

B. Residual signal disaggregation

In order to maximise the utility of the residual for diagnosis and prognosis, a modal analysis of MBT with respect to rotor shaft speed is performed. Fig.5 shows the joint distribution of main shaft RPM and the main bearing temperature, identified using a kernel density estimator [21],

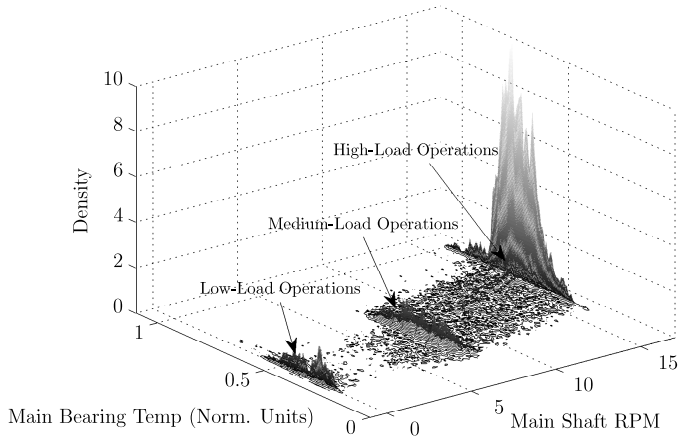


Fig. 5. Joint distribution of main shaft RPM and the main bearing temperature

Operating Region	Low-Load	Medium-Load	High-Load
RPM Range	0.1 - 2	7 - 9	15 - 16

TABLE I
MAIN BEARING OPERATING MODES: RPM RANGE

and indicates a number of discrete operating modes, which are documented in Table I.

It was found that a modified residual signal, consisting of a low-pass filtered (with an effective time constant of 33 hours) version of the ‘Low-load’ residual, gave optimum performance, in terms of the monotonicity and consistency of the MBT residual, as the main bearing failure mode evolved. A comparison of the filtered versions of the full residual, and the residual disaggregated by ‘Low-load’ operation, is shown in Fig.6.

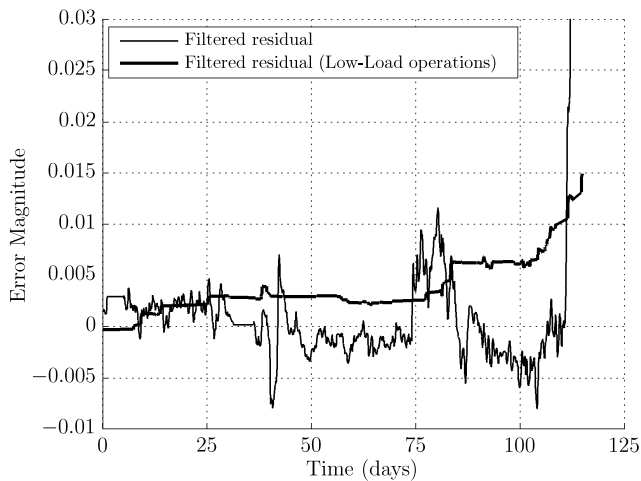


Fig. 6. Filtered residual signal by turbine operating mode

C. Fault threshold specification

Finally, in order to signal the onset of a fault, a threshold must now be placed on the filtered residual. For the low-load data, the residual distribution has a standard deviation (σ) of 0.0097. For a Gaussian distribution, the 99% confidence limits are defined by approx. $\pm 3\sigma$. Therefore, to provide a sufficient separation between the expected limits of ‘normal’ fault-free operation, a value of 0.004 ($> 4\sigma$) was chosen to define the threshold at which a fault condition is confirmed.

IV. PROGNOSTICS

Dynamic model-based approaches to prognostics are based upon estimating of the current level of degradation (the degradation state) and employing a model which describes the future evolution of the degradation process. In recent times, prognostic methods based upon recursive Bayesian filtering techniques are increasingly being applied to prognostic problems [22], [23], [24]. In particular, particle filtering provides a consistent framework to handle model non-linearities and potentially non-Gaussian noise processes.

Particle filtering, also known as Sequential Monte Carlo (SMC) methods [25], is a technique for implementing a recursive Bayesian filter via Monte Carlo simulations. The basic principle of particle filtering is to represent the *posterior* state PDF by a set of random samples or ‘particles’, each with an associated weight, and to compute estimates based on these samples and weights $\{x_k^{(i)}, w_k^{(i)}\}_{i=1}^{N_s}$. A set of particles are generated and recursively updated by a nonlinear process model (3) (which describes the evolution of the process under observation) and a measurement models (4), given the set of measurements, $z_{1:k} = (z_1, \dots, z_k)$, generated from the process.

$$x_k = f_k(x_{k-1}, \omega_k) \leftrightarrow p(x_k|x_{k-1}) \quad (3)$$

$$z_k = h_k(x_k, v_k) \leftrightarrow p(z_k|x_k) \quad (4)$$

A. Particle filters

The application of particle filtering for prognostic involves two distinct stages, *state estimation* and *long-term predictions*.

1) *State estimation*: In principle, the *posterior* state PDF $p(x_k|z_k)$ can be estimated recursively by performing two sequential steps, *prediction* and *update* [26]. Given the probability distribution $p(x_{k-1}|z_{1:k-1})$ at time t_{k-1} , the *prediction* step uses the system model (3) to obtain the *a priori* state PDF $p(x_k|z_{1:k-1})$, at time t_k .

$$p(x_k|z_{1:k-1}) = \int p(x_k|x_{k-1}, z_{1:k-1}) p(x_{k-1}|z_{1:k-1}) dx_{k-1} \quad (5)$$

Following the *prediction* step, the *update* step incorporates the latest measurement vector z_k , the *a priori* state PDF $p(x_k|z_{1:k-1})$ calculated in the *prediction* step, the *likelihood* function $p(z_k|x_k)$, and uses Bayes’ rule to estimate the *a posteriori* state PDF $p(x_k|z_{1:k})$ [26] as:

$$p(x_k|z_{1:k}) = \frac{p(z_k|x_k) p(x_k|z_{1:k-1})}{p(z_k|z_{1:k-1})} \quad (6)$$

Using particle filtering, the actual *a posteriori* state PDF is approximated as

$$p(x_k|z_{1:k}) \approx \sum_{i=1}^{N_s} w_k^{(i)} \delta(x_{0:k} - x_{0:k}^{(i)}) \quad (7)$$

where δ is the dirac-delta function, and (7) describes a discrete weighted approximation to the true *a posteriori* state distribution $p(x_k|z_{1:k})$ [26]. The principle of *importance sampling* [26] is used to update the particle weights at each iteration, where the formula for updating the particle weights is given by [26]

$$w_k^{(i)} = w_{k-1}^{(i)} \frac{p(z_k|x_k)p(x_k|x_{k-1})}{q(x_k|x_{0:k}, z_{1:k})} \quad (8)$$

where $q(x_k|x_{0:k}, z_{1:k})$ is the importance density [26], often chosen as the *a priori* PDF for the state, so that $q(x_k|x_{0:k}, z_{1:k}) = p(x_k|x_{k-1})$, which leads to a simplification of the weight update formula [26].

2) *Long Term Predictions*: Assuming that the current set of particles and weights $\{x_k^{(i)}, w_k^{(i)}\}_{i=1}^{N_s}$ are a good representation of the system state at time t_k , then the predicted state PDF at time t_{k+p} can be approximated by using the law of total probabilities [22], whereby

$$\hat{p}(\hat{x}_{k+p}|\hat{x}_{k:k+p-1}) \approx \sum_{i=1}^{N_s} w_{k+p-1}^{(i)} \hat{p}(\hat{x}_{k+p}^{(i)}|\hat{x}_{k+p-1}^{(i)}) \quad (9)$$

Once the projected path for each particle, $\hat{x}_{k+p}^{(i)}$, has been generated, and the time at which each particle enters the hazard zone (which defines an upper H_{ub} and lower H_{lb} bound range of values of the degradation state, at which time the system is considered to have reached the end of its serviceable life) has been identified, this information is then combined with the weight of each particle $w_k^{(i)}$ to generate a RUL PDF for the system. The RUL PDF can be computed as:

$$p_{ttf}(k+p) = \sum_{i=1}^{N_s} Pr(Failure|X = \hat{x}_{k+p}^{(i)}, H_{lb}, H_{ub}) \cdot w_{k+p}^{(i)} \quad (10)$$

where $p_{ttf}(k+p)$ is the probability of equipment failure at time t_{k+p} . The overall system RUL PDF is then approximated by the sum of the individual failure probabilities at each future time instant.

B. Multiple model particle filters

Two major sources of uncertainty in applying particle filtering to prognostics are model uncertainty (errors in model used to describe evolution of degradation process) and future load uncertainty. To address these challenges, a multiple model particle filtering approach is proposed [27] (Due to space limitations, a very brief description of the method is presented).

Using the available historical failure example, a set of candidate models, designed to approximate the potential behaviour of future failure examples, are first generated. Particle filtering, as described in Section IV-A, is then applied

for each candidate model. Initially, each candidate model is assigned equal weighting. Then, as a fault evolves, the plausibility that each candidate model is descriptive of the observed behaviour of the fault indicator is recursively estimated, and the weight of each candidate model is then updated to reflect how well each model describes the observed behaviour. The final RUL PDF is then generated as the weighted sum of the individual RUL PDFs generated by each candidate model.

C. Degradation process model

From previous experience [17], a useful model to describe the evolution of the main bearing degradation process, as described by the fault indicator signal, is:

$$x_k = x_{k-1} + \alpha_1 \exp\left[\frac{-\alpha_2/t_k}{t_k^2}\right] + \alpha_3 \exp[\alpha_4 t_k] + \omega_k \quad (11)$$

where x_k represents the degradation state at time t_k , the α_i values represent model parameters which can be tuned to fit the model to describe specific behaviour, and ω_k is a zero-mean Gaussian distribution representing the process noise term. The model was tuned to the available historical failure example, and from this a set of candidate approximating models were generated. The behaviour described by each of the generated candidate models is illustrated in Figure 7.

D. Application example

With just two turbines in the available data set with terminal faults, there is limited scope to validate our approach. Figure 7 illustrates the evolution of the RUL PDF for a single historical main bearing failure example. Note that, as the fault continues to evolve, the RUL PDF becomes more accurate and precise, as the behaviour of the degradation process evolves.

We note that the estimated parameters for the model in (11) are particular to each turbine and the variance of w_k in (11) provides a means to address uncertainty in future predictions. The more uncertain we are in the model, the greater the variance of w_k which has the effect of spreading out the predictions.

V. CONCLUSIONS

This paper presents a prognostic framework for the main bearing on commercial wind turbines using standard SCADA data, utilising a main bearing temperature model for residual generation. Since the residual models are local to each turbine, and the fault detection threshold is set well outside the 'normal' residual distribution, we can be reasonably confident that the fault detection threshold is robust. However, with the limited number of failure examples available in this study, the exact specification of the failure point or 'hazard zone' is more uncertain and requires further data to be robust. However, the prognostic engine employed provides useful and timely information to maintenance personnel; strong indication of failure is given with a 30 day lead time and the given probability density function gives an easy to interpret measure of confidence in the RUL estimate.

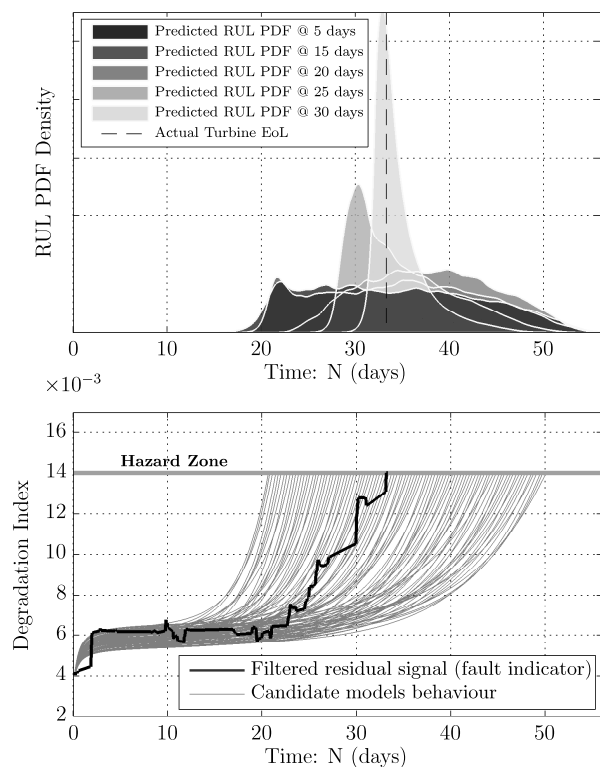


Fig. 7. Evolution of the RUL PDF for the main bearing of Turbine B and the multiple model projections from the prediction origin

REFERENCES

- [1] W. W. E. A. (WWEA), "World wind energy report 2010," World Wind Energy Association (WWEA), Tech. Rep., 2010.
- [2] D. McMillan and G. W. Ault, "Quantification of condition monitoring benefit for offshore wind turbines," *Wind Engineering*, vol. 31, pp. 267–285, 2007.
- [3] Z. Hameed, Y. Hong, Y. Cho, S. Ahn, and C. Song, "Condition monitoring and fault detection of wind turbines and related algorithms: A review," *Renewable and Sustainable Energy Reviews*, vol. 13, no. 1, pp. 1–39, 2009.
- [4] B. Lu, Y. Li, X. Wu, and Z. Yang, "A review of recent advances in wind turbine condition monitoring and fault diagnosis," in *Power Electronics and Machines in Wind Applications, 2009. PEMWA 2009. IEEE*, June 2009, pp. 1–7.
- [5] R. W. Hyers, J. G. McGowan, K. L. Sullivan, J. F. Manwell, and B. C. Syrett, "Condition monitoring and prognosis of utility scale wind turbines," *Energy Materials: Materials Science and Engineering for Energy Systems*, vol. 1, no. 3, pp. 187–203, 2006-09-01T00:00:00.
- [6] R. F. Orshagh, H. Lee, M. Watson, C. S. Byington, and J. Powers, "Advanced vibration monitoring for wind turbine health management," 2007.
- [7] G. Swiszczyk, A. Cruden, C. Booth, and W. Leithead, "A data acquisition platform for the development of a wind turbine condition monitoring system," in *Intl. Conf. on Condition Monitoring and Diagnosis*, April 2008, pp. 1358–1361.
- [8] S. Yang, W. Li, and C. Wang, "The intelligent fault diagnosis of wind turbine gearbox based on artificial neural network," in *Condition Monitoring and Diagnosis, 2008. CMD 2008. International Conference on*, April 2008, pp. 1327–1330.
- [9] W. Yang, P. Tavner, and M. Wilkinson, "Condition monitoring and fault diagnosis of a wind turbine synchronous generator drive train," *IET Renewable Power Generation*, vol. 3, no. 1, pp. 1–11, March 2009.
- [10] D. J. Lekou, F. Mouzakis, A. Anastasopoulos, and D. Kourousis, "Emerging techniques for health monitoring of wind turbine gearboxes and bearings," in *Proceedings of European Wind Energy Conference (EWEC)*, Marseille, March 2009.
- [11] K. Schroeder, W. Ecke, J. Apitz, E. Lembke, and G. Lenschow, "A fibre bragg grating sensor system monitors operational load in a wind turbine rotor blade," *Measurement Science and Technology*, vol. 17, no. 5, p. 1167, 2006.
- [12] O. Uluyol, G. Parthasarathy, W. Foslien, and K. Kim, "Power curve analytic for wind turbine performance monitoring and prognostics," in *Proc. Annual Conf. of the Prognostics and Health Management Soc.*, 2011.
- [13] P. Caselitz and J. Giebardt, "Rotor condition monitoring for improved operational safety of offshore wind energy converters," *Journal of Solar Energy Engineering*, vol. 127, no. 2, pp. 253–261, 2005.
- [14] A. Zaher, S. McArthur, D. Infield, and Y. Patel, "Online wind turbine fault detection through automated scada data analysis," *Wind Energy*, vol. 12, no. 6, pp. 574–593, 2009.
- [15] M. C. Garcia, M. A. Sanz-Bobi, and J. del Pico, "Simap: Intelligent system for predictive maintenance: Application to the health condition monitoring of a windturbine gearbox," *Computers in Industry*, vol. 57, no. 6, pp. 552–568, 2006.
- [16] P. Guo, D. Infield, and X. Yang, "Wind turbine generator condition-monitoring using temperature trend analysis," *Sustainable Energy, IEEE Transactions on*, vol. 3, no. 1, pp. 124–133, January 2012.
- [17] J. Butler and J. Ringwood, "Particle filters for remaining useful life estimation of abatement equipment used in semiconductor manufacturing," in *Proc. IEEE Conf. on Control and Fault-Tolerant Systems (SysTol)*, Nice, October 2010, pp. 436–441.
- [18] N. raper and H. Smith, *Applied Regression Analysis*, 2nd ed. Wiley, 1981.
- [19] E. Wiggelinkhuizen, T. Verbruggen, H. Braam, L. Rademakers, J. Xi-ang, and S. Watson, "Assessment of condition monitoring techniques for offshore wind farms," *Journal of Solar Energy Engineering*, vol. 130, no. 3, p. 031004, 2008.
- [20] M. E. Tipping and A. Faul, "Fast marginal likelihood maximisation for sparse bayesian models," in *Proc. 9th International Workshop on AI and Stats.*, 2003.
- [21] Z. I. Botev, J. F. Grotowski, and D. P. Kroese, "Kernel density estimation via diffusion," *The Annals of Statistics*, vol. 38, no. 5, pp. 2916–2957, 2010.
- [22] M. Orchard and G. Vachtsevanos, "A particle filtering based framework for on-line fault diagnosis and failure prognosis," *Trans. Inst. Meas. and Con.*, vol. 31, pp. 221–246, 2009.
- [23] M. Orchard, L. Tang, B. Saha, K. Goebel, and G. Vachtsevanos, "Risk-sensitive particle-filtering-based prognosis framework for estimation of remaining useful life in energy storage devices," *Studies in Informatics and Control*, vol. 19.
- [24] B. Saha and K. Goebel, "Modeling li-ion battery capacity depletion in a particle filtering framework," in *Ann. Conf. of Prognostics and Health Management Society*, 2009.
- [25] A. Doucet, S. Godsill, and C. Andrieu, "On sequential monte carlo sampling methods for bayesian filtering," *Statistics and Computing*, vol. 10, no. 3, pp. 197–208, 2000.
- [26] M. S. Arulampalam, S. Maskell, N. Gordon, and T. Clapp, "A tutorial on particle filters for online nonlinear/non-Gaussian bayesian tracking," *IEEE Trans. on Sig. Proc.*, vol. 50, no. 2, pp. 174–188, February 2002.
- [27] L. Tang, G. J. Kacprzyński, K. Goebel, and G. Vachtsevanos, "Methodologies for uncertainty management in prognostics," in *Proc. IEEE Conf. on Aerospace*, March 2009, pp. 1–12.